CrossMark

A Comparative Study on Activated Carbons Derived from a Broad Range of Agro-industrial Wastes in Removal of Large-Molecular-Size Organic Pollutants in Aqueous Phase

G. J. F. Cruz · L. Matějová · M. Pirilä · K. Ainassaari ·
C. A. Canepa · J. Solis · J.F. Cruz · O. Šolcová ·
R. L. Keiski

Abstract Microporous–mesoporous activated carbons from five different types of agro-industrial wastes were produced using chemical activation with $ZnCl_2$ and carbonization at mild conditions of 600 °C, comprehensively characterized and investigated for removal of methylene blue (MB) in aqueous solution, a model large-molecular-size organic pollutant. The external part of the mango pit (mango seed husk) was used for the production of activated carbon (AC) for the first time. Despite that the raw agro-materials exhibited significantly different porosity, all activated carbons produced possessed well-developed microporous–mesoporous structures showing high surface areas and micropore volumes. Further, it was revealed that the pore size distribution of raw agro-material is a more important property in development of microporous–mesoporous structure of produced ACs than their overall porosity. All activated carbons produced adsorbed MB, reaching in most cases 100 % removal from the aqueous phase. Adsorption data were fitted well to a pseudo-second-order kinetic model. For MB adsorption, the mesoporosity and the ratio of micropores accessible for MB were the key factors since there exists the size-selectivity effect on MB adsorption due to MB molecular dimensions. The molecular dimensions of MB were estimated via DFT calculations to $1.66 \times 0.82 \times 0.54$ nm, and this parameter was correlated with determined micropore size distributions of activated carbons.

Keywords Agro-industrial biomass · $ZnCl_2$ · Activated carbon · Large-molecular-size pollutant · Adsorption · DFT

G. J. F. Cruz · C. A. Canepa
Facultad de Ciencias Agrarias, Laboratorio de Análisis Ambiental, Universidad Nacional de Tumbes, Av. Universitaria s/n, Campus Universitario, Pampa Grande, Tumbes, Peru

L. Matějová (✉) · O. Šolcová
Department of Catalysis and Reaction Engineering, Institute of Chemical Process Fundamentals of the CAS, v. v. i, Rozvojová 135, 165 02 Prague, Czech Republic
e-mail: matejova@icpf.cas.cz

M. Pirilä · K. Ainassaari · R. L. Keiski
Faculty of Technology, Environmental and Chemical Engineering, University of Oulu, P.O. Box 4300, 90014 Oulu, Finland

J. Solis
Facultad de Ciencias, Laboratorio de Materiales Funcionales, Universidad Nacional de Ingeniería, Av. Tupac Amaru 210, Lima 25, Peru

J. Cruz
Departamento de Ingeniería Química, Universidad Nacional de Piura, Campus Universitario s/n, Urb. Miraflores, Piura, Peru

Abbreviations

S_{BET}	specific surface area calculated according to the classical BET theory (m^2/g)
S_{meso}	mesopore surface area calculated according to the modified BET equation (m^2/g)
$V_{intruse}$	pore volume determined by high-pressure mercury intrusion (cm^3/g)

V_{micro}	micropore volume calculated according to the modified BET equation (mm^3_{liq}/g)
V_{net}	net pore volume determined from the nitrogen adsorption isotherm at maximum p/p_0 (~0.9900) (mm^3_{liq}/g)
C_{modif}	adsorption constant in the first layer calculated according to the modified BET equation (−)
C_0	initial concentration of adsorbate in solution (mg/l)
C_t	adsorbate concentration in solution at time t (mg/l)
H	initial adsorption rate as q_t/t approaches 0 (mg/g min)
k_2	pseudo-second-order rate constant mg h)/mg h)
m_{AC}	mass of activated carbon mg h))
q_e	calculated equilibrium adsorption capacity (mg/g)
q_t	amount adsorbed at time t (mg/g)
t	adsorption time (h)
V	total volume of solution (l)
CPH-RM	cocoa pod husk raw material
CH-RM	coffee husk raw material
CC-RM	corncob raw material
MSIP-RM	internal part of the mango pit (mango seed) raw material
MSEP-RM	external part of the mango pit (mango seed husk) raw material
CPH-AC	cocoa pod husk-derived activated carbon
CH-AC	coffee husk-derived activated carbon
CC-AC	corncob-derived activated carbon
MSIP-AC	internal part of the mango pit (mango seed)-derived activated carbon
MSEP-AC	external part of the mango pit (mango seed husk)-derived activated carbon

Greek Letters

ε	porosity of material (%)
ρ_{Hg}	bulk density of material mg h)/cm^3)
ρ_{He}	skeletal density of material mg h)/cm^3)

1 Introduction

Coffee (*Coffea arabica* L.), cacao (*Theobroma cacao*), mango (*Manguifera indica*), and corn (*Zea mays*) are

four of the most promising agriculture products in Peru because of their high production levels, possibilities for exporting, and/or their alternatives for processing that give them aggregated value. Those raw materials are processed in primary and/or secondary levels, generating significant amounts of wastes that are usually composed of organic matter with different biodegradability. Despite the different alternatives to use them, only a fraction is recycled as animal food, in the production of organic fertilizers, or in the production of energy. The rest is disposed in illegal or legal dumps or burnt, generating greenhouse gases (such as CO_2 and CO) and particles and impacting the surrounding environment. The amount of waste produced by agro-industrial activities in Peru is excessive. Thus, for example in the case of coffee, the husk may represent 12 wt.% based on dry weight of the whole coffee bean; for mango, around 24 wt. % of the whole fruit is a husk, 60 wt. % is a pulp, and 16 wt.% is a pit (7 wt. % the pit external part and 9 wt. % the pit internal part); for cocoa, cocoa pod husk can represent from 70 to 75 wt. % of the whole weight of the pod; and corn grains constitute only 15 wt. % of the whole corn (Sych et al. 2012), meaning that 85 wt. % is a corncob and husk. Taking as a reference the agricultural production of the year 2012 (Minagri 2013) and considering that 50 wt. % of this production is processed in different levels (the rest is directly sold), the amount of agro-industrial residues generated in 2012 could be around 18,870 tons of coffee husk, 21,761 tons of husk, 15,000 tons of mango pits, 21,875 tons of cocoa pod, and 1,648,405 tons between husk and corncob.

One of the feasible alternatives to recycle such residues, according to their content of lignocellulosic compounds, is as precursors for the production of activated carbon (AC), a material with a high surface area suitable for adsorption and catalytic applications. The traditional materials for activated carbon production (such as wood, lignin, coal, etc.) could be replaced for those cheap and renewable residues to reduce costs and improve the sustainability of the production process. The residues mentioned above have been studied in different experimental conditions around the world: cocoa pod husk (Cruz et al. 2012; Ahmad et al. 2012; Theivarasu and Mylsamy 2010; Bello et al. 2011; Fisal et al. 2011), coffee husk (Oliveira et al. 2009; Ahmad and Rahman 2011), mango pits (Kwaghger and Ibrahim 2013; Akpen et al. 2011), and corncob (Song et al. 2013; Bagheri and Abedi 2009; Tsai et al. 1998) for the removal of different organic and inorganic compounds in aqueous solutions.

Despite that there is a wide range of studies about the production of activated carbons for different water treatment applications, the interest to produce activated carbon from cheap and renewable raw materials showing a high surface area and special properties for specific application is still increasing. One of the desirable special features in activated carbon porous structure to be used as an adsorbent is the development of microporosity as well as mesoporosity, simply said a compromise between them, depending on the application needs. The accessibility of the organic molecules to the micropores can be limited (Dias et al. 2007). Thus, the high mesoporosity plays an important role in the adsorption of organic molecules, metal–organic molecules, or hydrated metallic ions in aqueous-phase systems. Besides the mesopores allowing pollutants to access the micropores, the mesopores are themselves an available area with active sites for pollutant adsorption. The equilibrated balance between the preparation of high-quality adsorbents, their costs, and environmental issues solved is very important for designing the systems for activated carbon production. The amount of chemical activation, use of high temperature during carbonization, and use of different basic or acid compounds in high concentrations could increase production costs and make difficult to scale up the process; therefore, it is required to produce high-quality microporous–mesoporous activated carbons with less production inputs, energy, etc. Different activation agents are used to produce activated carbon, however, $ZnCl_2$ has been widely used based on its effectiveness to build a well-developed microporous–mesoporous structure of activated carbon at moderate activation temperatures and reach high yields compared to other chemical activators (Azevedo et al. 2007). Obviously, $ZnCl_2$ has some environmental implications, but it is a problem of all chemical activators.

This study aimed to produce and characterize microporous–mesoporous activated carbons from a broader range of agro-industrial wastes, using the chemical activation with $ZnCl_2$ and carbonization at mild conditions, and investigate them for the removal of model large-molecular-size organic pollutant in aqueous phase. The main goal was to reveal the key material properties influencing the ACs adsorption performance for removal of organic pollutants via following new approaches and methodologies:

- To use a simple "activation–carbonization" method to produce activated carbons with microporous–mesoporous structure

- To use a novel raw material (external part of the mango pit—mango seed husk) in activated carbon production

- To use high-pressure mercury porosimetry and helium pycnometry to characterize also the raw lignocellulosic precursors in order to reveal the possible correlation between the porosity of raw agro-material and the quality of activated carbons produced

- To apply the modified BET equation to calculate textural properties of the activated carbons produced such as mesopore surface area, S_{meso}, and micropore volume, V_{micro}, since the specific surface area, S_{BET}, is not a correct parameter used for the characterization of mesoporous materials containing micropores

- To reveal the key properties determining the ACs' adsorption performance in the removal of large-molecular-size organic pollutants, namely, methylene blue. In order to prove or disprove the possibility of larger organic pollutant being adsorbed in the micropores or not, the molecular dimensions of the model organic pollutant (methylene blue) were estimated via DFT calculations and correlated with the textural properties of produced ACs

2 Materials and Methods

2.1 Materials

Cocoa (*T. cacao*) pod husk (CPH-RM), the internal and external parts of mango (*M. indica*) pits (MSIP-RM and MSEP-RM, respectively), coffee (*C. arabica* L.) husk (CH-RM), and corn (*Z. mays*) cob (CC-RM) were collected from different agro-industrial factories and agricultural areas in two cities in the north of Peru, Piura and Tumbes.

2.2 Reagents

$ZnCl_2$ (EMSURE ACS, ISO, Reag. Ph Eur, Merck) was used as the chemical activator. Methylene blue (Certistain C.I. 52015, Merck) was used for preparing a 1000-mg/l methylene blue stock solution, which was utilized for the preparation of other solutions for adsorption experiments and the calibration of a spectrophotometer.

2.3 Characterization of the Raw Agro-materials

An overview on ash and carbonaceous compound contents in the raw materials used, studied previously by different authors, is summarized in Table 1.

The bulk density (ρ_{Hg}), the mercury intrusion pore volume $(V_{intruse})$, and the skeletal density (ρ_{He}) of the processed raw precursors were determined by high-pressure mercury porosimetry and helium pycnometry using AutoPore III (Micromeritics, USA) and AccuPyc II 1340 pycnometer (Micromeritics, USA), respectively. Prior to the measurements, the precursors received as non-crushed raw materials were dried in an oven at 105 °C for several days to remove physisorbed moisture. For each raw material, high-pressure mercury porosimetry measurement was carried out at least twice in order to evaluate an average value of porosity because of the inhomogeneity of raw materials. Porosity (ε in %) of the raw materials was calculated according to the equation $\varepsilon = (1 - \rho_{Hg}/\rho_{He}) * 100$.

Nitrogen physisorption at 77 K was measured in order to determine the specific surface area, S_{BET}, of raw materials. Prior to the nitrogen physisorption measurements, the sieved (particle size 0.5–1 mm) raw agro-materials were firstly dried in an oven at 105 °C under ambient pressure for 72 h and then degassed at a temperature of 105 °C for 48 h under vacuum less than 1 Pa. No changes in the appearance of raw agro-materials were observed during the drying procedure, thus assuming no influence on the textural properties of investigated materials. The nitrogen physisorption measurements at 77 K were performed on ASAP 2050 (Micromeritics, USA). S_{BET} was calculated according to the classical Brunauer–Emmett–Teller (BET) theory for the p/p_0 range=0.05–0.25 (Brunauer et al. 1938).

2.4 Production of Activated Carbons

CPH-RM and MSIP-RM as fresh precursors were repeatedly washed with tap water in order to remove fruit pulp remnants and to avoid undesirable reactions during activation and pyrolysis. MSEP-RM, CH-RM, and CC-RM were used without being washed. Subsequently, all raw materials were dried at 100 °C until they achieved a constant weight, then they were ground, and the 0.5–1 mm particle size fraction was separated. $ZnCl_2$ was used in a weight ratio of 1/1 using impregnation in dry conditions.

The samples of raw agro-materials were put in a metallic reactor to be pyrolyzed at 600 °C in a furnace. This temperature level is enough to thermally degrade the total amount of lignocellulosic compounds, considering that lignin has a degradation temperature between 280 and 500 °C, cellulose between 240 and 350 °C, and hemicellulose between 200 and 260 °C (Mohan et al. 2006). A heating rate of 10 °C/min was applied to reach the final pyrolysis temperature, at which the samples were kept for 2 h and then cooled down to room temperature. The whole process of carbonization was done under nitrogen atmosphere at a flow of ~100 ml/min. After the pyrolysis, ACs produced were washed with a solution of HCl 0.15 M (in a proportion 10 ml of solution per gram of AC) and then washed repeatedly and exhaustively with room temperature distilled water until the washed solution reached a pH of 6–6.5. Finally, all ACs

Table 1 Characterization of the agro-industrial wastes used as raw materials for activated carbon production

Raw material	Ash content (wt.%)	Starch (wt.%)	Cellulose (wt.%)	Hemi-cellulose (wt.%)	Lignin (wt.%)	Total lignocellulosic material (wt.%)	Reference
MSEP-RM	0.58	0.2	39.4	15.6	5.6	60.6	Elizalde-González and Hernandez-Montoya (2007)
MSIP-RM	1.10	18.0	14.5	52.4	3.8	70.7	Elizalde-González and Hernandez-Montoya (2007)
CPH-RM	12.3	–	35.4	37.0	14.7	87.12	Hatta (2013)
CH-RM	6.2	–	25.5	29.7	23.7	78.9	Bekalo and Reinhardt (2010)
CC-RM	0.2	–	36.3	42.8	9.3	88.4	Sun and Webley (2010)

– no data available

were dried at 100 °C overnight, ground, and sieved with a mesh of 0.25 mm in grid size.

2.5 Characterization of Activated Carbons Produced

Textural analyses were carried out in order to well characterize the obtained porous structure of activated carbons.

The weight loss (wt. %) of the activated carbons production was calculated by using the following equation:

$$WL(\text{wt.}\%) = \frac{W_I - W_F}{W_I} \times 100 \tag{1}$$

where WL is the weight loss (wt. %), W_F is the final weight on a chemical-free basis (after final washing) and W_I is the initial raw material weight used before the addition of the chemical activation agent. The chemical recovery (wt. %) was calculated by:

$$CR(\text{wt.}\%) = \frac{W_{BW} - W_{AW}}{W_C} \times 100 \tag{2}$$

where CR is the chemical recovery (wt. %), W_{BW} and W_{AW} are the weight of the adsorbent before and after washing, respectively, and W_C is the weight of the chemical activation agent used.

Nitrogen physisorption was measured in order to determine the textural parameters of the activated carbons produced. The nitrogen physisorption measurements at 77 K were performed on a Gemini VII 2390 Surface Area Analyzer (Micromeritics, USA). The specific surface area, S_{BET}, was calculated according to the classical BET theory for the p/p_0 range=0.05–0.25 (Brunauer et al. 1938). As the specific surface area, S_{BET}, is not a correct parameter in the case of mesoporous solids containing micropores mg h)regg and Sing 1982), the mesopore surface area, S_{meso}, and the micropore volume, V_{micro}, were also evaluated based on the modified BET equation with the C_{modif} constant (Schneider 1995; Lecloux and Pirard 1979). The results from the modified BET equation were additionally also correlated with the results from the t-plot method using Lecloux–Pirard standard isotherm and considering the estimated C_{modif}. The net pore volume, V_{net}, was determined from the nitrogen adsorption isotherm at maximum p/p_0 (~0.9900). The mesopore size distribution was evaluated from the desorption branch of the nitrogen adsorption–desorption isotherm by the Barrett–

Joyner–Halenda method (Barrett et al. 1951), via the Roberts algorithm (Roberts 1967), using the carbon standard isotherm and the assumption of the slit-pore geometry. The micropore size distribution of the activated carbons produced was evaluated from the low-pressure part of the nitrogen adsorption isotherms ($10^{-7} < p/p_0 < 0.05$) obtained with an apparatus ASAP2020 (Micromeritics, USA) using the Horvath–Kawazoe solution for the slit-pore geometry of carbonaceous materials (Horvath and Kawazoe 1983).

SEM images were obtained using a FEI Quanta 200 plus scanning electron microscope equipped with Oxford Instruments INCA-X-act EDS detector.

2.6 Adsorption Experiments

2.6.1 Methylene Blue Adsorption

Adsorption experiments were carried out to test methylene blue (MB) adsorption capacity of activated carbons produced. The experiments were conducted without pH adjustment (the initial pH level was between 5.5 and 6.5) and at room temperature between 20 and 25 °C. The activated carbon concentration was 0.5 g/l, and the initial MB concentration was 50 mg/l in a 200-ml batch. The solutions were shaken in a magnetic stirrer during the experiments. Filtered liquid aliquots were extracted at the beginning and at different times between 5 and 150 min. The MB concentration was determined at the 660-nm wavelength on a Spectroquant Pharo 300 UV–vis spectrophotometer (Merck).

2.6.2 Adsorption Kinetic Model

A pseudo-second-order kinetic model (Ho and McKay 1999) was applied to describe the behavior of MB adsorption data. The integral form of that model can be written as follows:

$$\frac{t}{q_e} = \frac{1}{k_2 q_e^2} + \frac{t}{q_e} \tag{3}$$

where t is the adsorption time (min), q_t is the amount adsorbed at time t (mg of adsorbate/g of activated carbon), k_2 is the pseudo-second-order rate constant mg h)/mg min), and q_e is the calculated equilibrium adsorption capacity (mg of adsorbate/g of activated

carbon). The initial adsorption rate as q_t/t approaches 0; h (mg of adsorbate/g of adsorbent min) was calculated according to the following equation:

$$h = k_2 \cdot q_e^2 \tag{4}$$

The amount of adsorbate adsorbed at time t was calculated by using the following mass balance equation:

$$q_t = \frac{(C_0 - C_t)V}{m_{AC}} \tag{5}$$

where C_0 and C_t are the initial adsorbate concentration and the adsorbate concentration in solution at time t (mg/l), respectively, V is the total volume of solution (l) and m_{AC} is the mass of activated carbon (g).

2.7 Computational Methodology (DFT Calculations)

The molecule optimization for methylene blue (MB) was performed with Gaussian 03 package (Frisch et al. 2004) with B3LYP (Becke 1993; Lee et al. 1988) hybrid functional and a 6-31+G(d,p) basis set. The vibrational analysis showed that the structure corresponds to local minima in potential energy surface. Wave functions from optimized structure were used for the visualization of the contour map of electrostatic potentials by the Multiwfn program (Lu and Chen 2012). Vander Waals volume was computed by Monte Carlo method as implemented in the Multiwfn program. The molecular dimensions in x, y, and z-coordinate axis were evaluated based on the graphical output of the Multiwfn program as the maximum values of vnW surface in individual coordinate axis.

3 Results and Discussion

3.1 Raw Agro-materials Characterization

The results from high-pressure mercury porosimetry and helium pycnometry measurements (Table 2) obtained for individual raw materials reveal that investigated raw materials show significantly different porosity in the broad range of 15–65 %. From all agro-industrial wastes, CC-RM is the most porous material ($\varepsilon \sim 65 \pm 1$ %) and CH-RM is the least porous material ($\varepsilon \sim 15 \pm 1$ %). Concerning raw materials from mango seed, MSEP-RM was about 10 % more porous than MSIP-RM. The overall order in porosity of raw materials was as follows: CC-RM>CPH-RM>MSEP-RM>MSIP-RM>CH-RM. The fact that the precursor raw material has higher porosity could be important since higher porosity of the raw material may mean higher surface area being in the contact with activation agent, improving the overall activation process and thus resulting in activated carbons with well-developed microporous–mesoporous structure possessing higher surface areas.

According to the repeated high-pressure mercury porosimetry measurements (Fig. 1; Table 2) MSEP-RM, CH-RM, and CC-RM are relatively homogeneous materials and have regular porous structure with pore sizes of 0.002–4 μm contrary to CPH-RM and MSIP-RM which are either inhomogeneous (CPH-RM) or homogeneous with irregular porous structure (MSIP-RM). From the PSD curves in Fig. 1, it is evident that CC-RM in contrast to other raw precursor materials has dominantly larger uniform pores. MSEP-RM, MSIP-RM, CPH-RM, and CH-RM show pores of wide range of sizes. From Table 2, it can be also seen that all raw

Table 2 The density and porosity of agro-industrial wastes as-received and the specific surface area of agro-industrial wastes sieved to particle size fraction of 0.5–1 mm

Raw material	ρ_{He} (g/cm^3)	ρ_{Hg} (g/cm^3)	$V_{intruse}$ (cm^3/g)	ε (%)	S_{BET} (m^2/g)
MSEP-RM	1.39	0.89	0.40	38±2	0.29
		0.83	0.56		
MSIP-RM	1.40	1.04	0.32	27±1	0.31
		1.02	0.30		
CPH-RM	1.43	0.53	0.39	48±16	0.44
		0.95	0.40		
CH-RM	1.33	1.14	0.15	15±1	0.40
		1.13	0.19		
CC-RM	1.28	0.45	1.40	65±1	–
		0.46	1.56		

– no data available

Fig. 1 Pore size distributions of raw agro-industrial wastes determined by high-pressure mercury porosimetry: **a** MSEP-RM, **b** MSIP-RM, **c** CPH-RM, **d** CH-RM, and **e** CC-RM
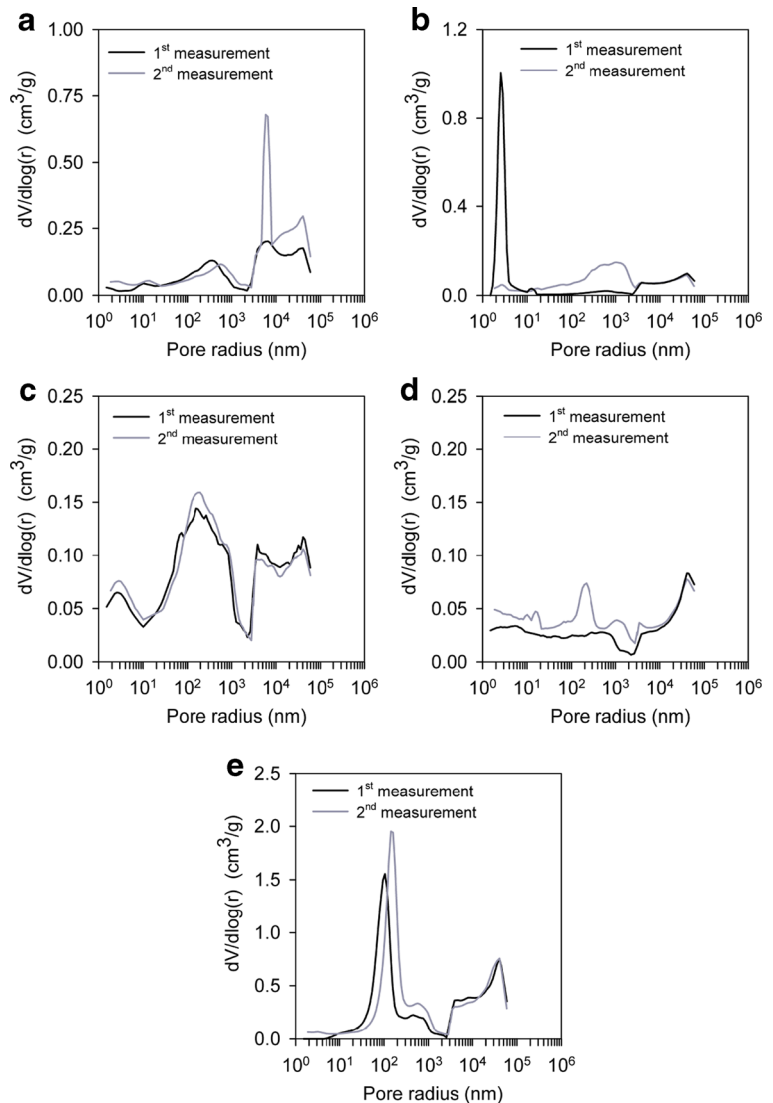
materials show very low surface areas, within the range 0.29–0.44 m^2/g.

3.2 Activated Carbon Production and Characterization

It is important to notice than $ZnCl_2$ is a hydroscopic compound, and during impregnation in dry conditions it adsorbs water from the surrounding. This highly concentrated $ZnCl_2$ solution accesses the pores of the raw precursor, and two phenomena may occur: (1) since $ZnCl_2$ is a salt, water inside cells is released to the $ZnCl_2$ solution because of the osmotic pressure, dehydrating the cells and thus increasing the porosity of the raw precursors; (2) water in the pores of the raw precursor (could be physisorbed water as well) is mixed with the $ZnCl_2$ solution inside the pores. Those phenomena may occur simultaneously and improve the contact between $ZnCl_2$ and a raw material.

Table 3 displays the weight losses obtained for the activated carbons produced. Despite the same conditions during the preparation sequence, the activated carbons exhibit different weight loss levels. Since cellulose, hemicellulose, and lignin show different volatilization, the differences in the levels of weight loss might depend on the proportion of these lignocellulosic compounds in each raw material. On the other hand,

Table 3 The weight loss and chemical recovery during activation and carbonization processes in the activated carbons productions

Activated carbon	Weight loss (wt. %)	Chemical recovery (wt. %)
MSEP-AC	49.7	69.8
MSIP-AC	48.7	63.2
CPH-AC	55.1	63.3
CH-AC	49.7	70.9
CC-AC	45.4	63.1

Fig. 2 Pictures of the produced activated carbon: a MSEP-AC, b MSIP-AC, c CPH-AC, d CH-AC, and e CC-AC

different reaction products formed during the process of carbonization and activation in inert atmosphere could be more volatile than others for different raw materials and could affect the weight loss. $ZnCl_2$ is considered as a Lewis acid and promotes aromatic condensation reactions. Molecular hydrogen evolves from the hydroaromatic structure of the raw material during the pyrolysis and produces free sites for reactions. Different cross-linking or aromatization reactions may take place between adjacent molecules and stabilize molecules that are usually volatiles (Ahmadpour and Do 1997). It may occur in different levels during the pyrolysis, depending on the raw precursor composition.

The $ZnCl_2$ recovery for the production of different activated carbons was higher than 63.1 wt. %, reaching up to 70.9 wt. % in the case of CH-AC (Table 3). The high chemical activation recovery might be due to the high water solubility of zinc salts left in the carbon mass (Ahmadpour and Do 1997).

All activated carbons produced were granular (Fig. 2). Despite the same initial particle size of the raw materials, the particle size of activated carbons produced is different depending on the type of raw material. The granular structure of the activated carbons produced is important due to the fact that these materials should be directly used for designing of a water or wastewater treatment unit. Using the granular activated carbon in water and wastewater treatment applications reduces the loss of material and enhances the recovery and the regeneration of adsorbent during the post-treatment.

It is worth to discuss the aspect of large-size compact particles in the activated carbons produced (Fig. 2). Nieto and Rangel (2013) studied, using an environmental scanning electron microscope, the $ZnCl_2$ activation mechanism during the activation and carbonization of
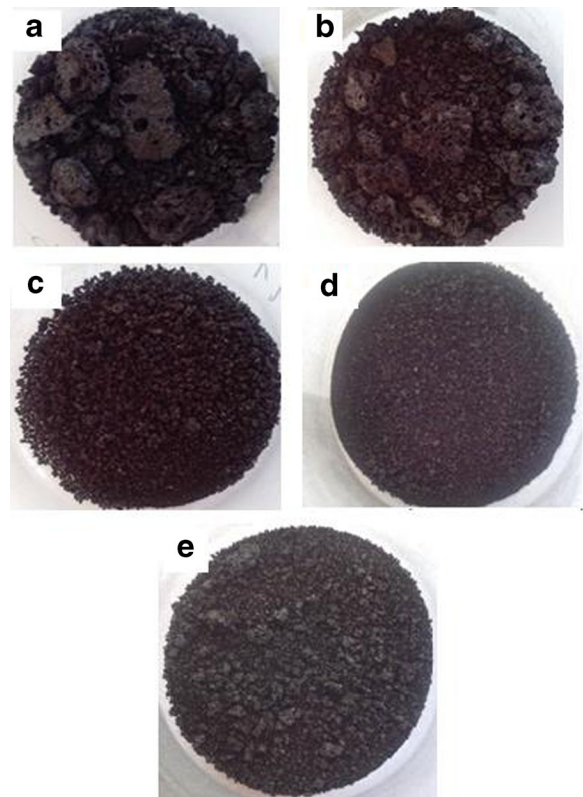
agave bagasse. They identified that a molten phase is involved during these processes. That plastic phase might be responsible for the formation of $ZnCl_2$-activated carbon of compact large particles, which makes this type of activation favorable with concerning its application.

In general, all analyzed activated carbons showed a high surface area. CPH-AC, CH-AC, and CC-AC showed S_{BET} higher than 1100 m^2/g; MSIP-AC had slightly lower surface area than MSEP-AC (Table 4). Considering the fact that the specific surface area, S_{BET}, is not principally a well-evaluated textural parameter in the case of mesoporous solids containing micropores mg h)regg and Sing 1982), this parameter will be used in further discussion only as information for comparison of the quality of activated carbons produced by other authors.

Oliveira et al. (2009) found that the S_{BET} for CH-AC, activated with $ZnCl_2$, was 1522 m^2/g, a value higher than the result found in this study. The reason of this result is the pyrolysis time which was only 2 h in this

Table 4 Textural parameters of the activated carbons produced determined from nitrogen physisorption

Sample	S_{BET} (m^2/g)	S_{meso} (m^2/g)	V_{micro} (mm$^3_{liq}$/g)	V_{net} (mm$^3_{liq}$/g)	V_{micro}/V_{net} (%)	C_{modif} (−)
MSEP-AC	939	504	221	602	37	19.0
MSIP-AC	1094	561	266	691	38	19.0
CPH-AC	1162	503	322	726	44	23.9
CH-AC	1135	518	305	732	42	20.8
CC-AC	1121	618	250	657	38	21.5

study compared to the Oliveira et al. study where the pyrolysis time used was 3 h. A longer pyrolysis time permits to produce activated carbons with higher surface area, but it leads to weight loss. Ahmad and Rahman (2011) used NaOH as the chemical activation agent in the production of CH-AC, and they obtained a material with S_{BET} of 745.17 m^2/g.

Various authors have produced CPH-AC with different S_{BET}, but the surface area of CPH-AC achieved in the present study (~1162 m^2/g) is higher than those found by other authors: Ahmad et al. (2012) 85.09 m^2/g, Bello et al. (2011) 502.7 m^2/g, and Fisal et al. (2011) 248 m^2/g.

Kwaghger and Ibrahim (2013) used HCl as the chemical activation agent to prepare MSIP-AC showing high S_{BET} (1142.3 m^2/g); MSIP-AC from this study shows similar specific surface area (i.e., 1094 m^2/g). No references were found to compare the S_{BET} of MSEP-AC.

Concerning CC-AC, Song et al. (2013) produced CC-AC with S_{BET} close to 1600 m^2/g using, sequentially, physical and chemical activation with steam and a saturated KOH solution, respectively. Bagheri and Abedi (2009) obtained CC-AC with S_{BET} of 1320 m^2/g using KOH as well, but using agent/raw material impregnation ratio of 2/1. Tsai et al. (1998) elaborated CC-AC under various conditions; however, also using similar conditions as in this study (activator agent=ZnCl$_2$, activated agent/raw material ratio =1/1, pyrolysis time=2 h and pyrolysis temperature=600 °C), they obtained CC-AC with S_{BET} of ~791 m^2/g. In this study, CC-AC with higher surface area was prepared.

The shape of nitrogen adsorption–desorption isotherms of activated carbons produced in this study (Fig. 3a–c) corresponds basically to the type I isotherm according to the IUPAC classification mg h)regg and Sing 1982), typical for microporous materials. Besides that, the isotherms include hysteresis loops at higher relative pressures, which are typical for the IV type

IUPAC isotherm, indicating the presence of mesoporous structure. According to Fig. 3 and Table 4, all activated carbons produced from lignocellulosic agro-industrial wastes exhibit a well-developed microporous–mesoporous structure. However, several significant differences can be seen. CC-AC shows significantly higher mesopores surface area (~618 m^2/g) than other ACs (503–561 m^2/g), but not so high micropore volume. Concerning mango seed-produced ACs, MSIP-AC shows very similar porous structure morphology as MSEP-AC but is slightly more porous. CPH-AC and CH-AC also possess practically the same porous structure morphology. The micropore volume of individual ACs is decreasing in following order: CPH-AC~CH-AC>MSIP-AC~CC-AC>MSEP-AC. CC-AC comprises the most uniform mesopores. Micropore size distributions (Fig. 4) of CPH-AC, MSIP-AC, MSEP-AC, and CH-AC reveal that activated carbons produced have very similar irregular microporous structure. ACs comprise smaller and larger micropores with pore sizes 0.4–0.45 and above ~0.48 nm, respectively. In general, the pore size distributions of the activated carbons might be the determining parameter in the case of polluted water and wastewater treatment because of the possible fast access for low and high molecular weight molecules of pollutants through macropores and mesopores to reach micropores, improving thus the adsorption properties of developed adsorbent mg h)aliatsatou et al. 2001).

According to Liou (2010), the acidic washing of the activated carbons causes the mesopore volume and mesopore surface area increase due to pore widening when the acid solution removes the ash inside activated carbons. It is important to notice than high ratios of activator agent/raw material (more than 1/1) might increase the surface area of the activated carbons (Hu et al. 2003). However, these conditions increase the process costs and the risk of higher production of zinc that could cause more serious environmental and health impact.

Fig. 3 a–c Measured nitrogen adsorption–desorption isotherms and d–f evaluated pore size distributions of activated carbons produced
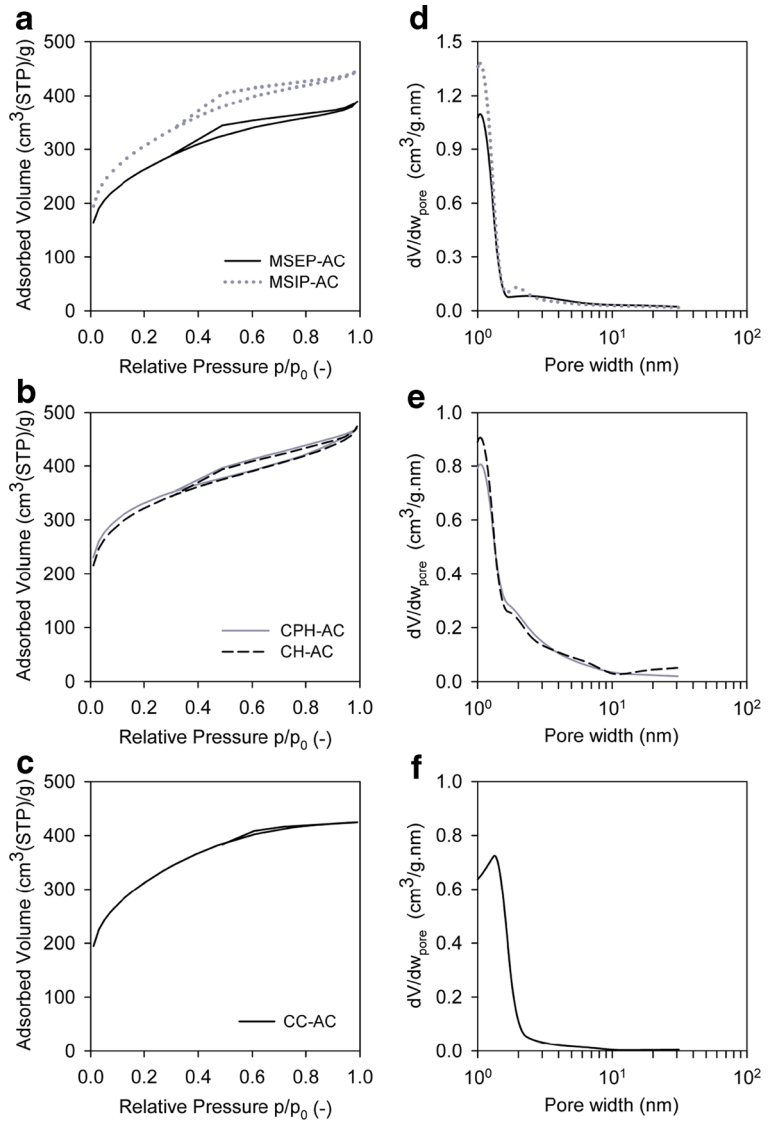
Linear regression models were conducted in order to study the relationship between the porosity (ε) of the raw material and the S_{meso} and V_{micro} of the activated carbons produced. The calculated correlation

Fig. 4 Evaluated micropore size distributions of activated carbons produced. Data for CC-AC are not available
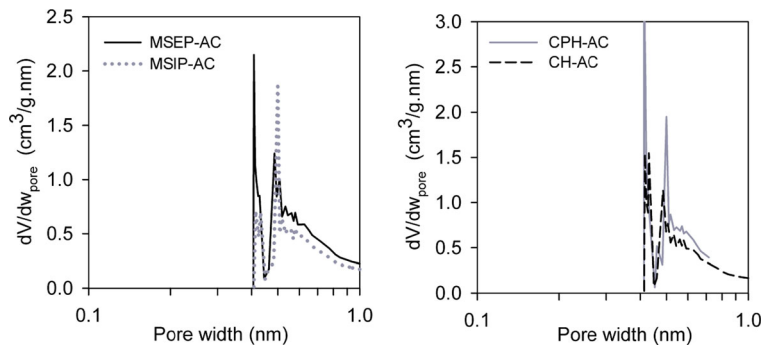
coefficients of the models were middle in the case of relationship between ε and S_{meso} (0.53) and low in the case of ε and V_{micro} (0.25). Therefore, it can be proved that there is no direct relationship between the porosity of original raw agro-material and the textural properties such as a surface area or micropore volume of developed ACs. On the other side, it is evident that the utilization of a raw agro-material possessing dominantly uniform macropores of ~300 nm pore size and of large volume (Fig. 1e; Table 2) results in AC showing the well-developed mesoporous structure, having the highest mesopore surface area and channel-like pore morphology (Table 4; Figs. 3f and 5e), which is the case of CC-RM. Thus, it can be concluded that the pore size distribution of raw agro-material plays a more important role in developing of microporous–mesoporous ACs than

their overall porosity. It can affect the level of interaction of an activation agent with a lignocellulosic material. In general, the raw materials showing a wide range of pore sizes and higher ratio of larger pores within a mesoporous–macroporous structure allow developing of the activated carbons with high surface areas.

Based on the SEM images of ACs (Fig. 5), it is possible to see pores with different sizes, including smaller pores inside larger pores. This shows that in the adsorption process, the access to the porous structure might be available for pollutants dissolved or carried by water or wastewater. The nice channel-like mesoporous–macroporous structure is visible for CC-AC (Fig. 5e). Otherwise, in other cases, the pores are irregular, not perfectly circular, and heterogeneous with different sizes. Some impurities were identified in the SEM

Fig. 5 SEM micrographs of **a** MSEP-AC, **b** MSIP-AC, **c** CPH-AC, **d** CH-AC, and **e** CC-AC
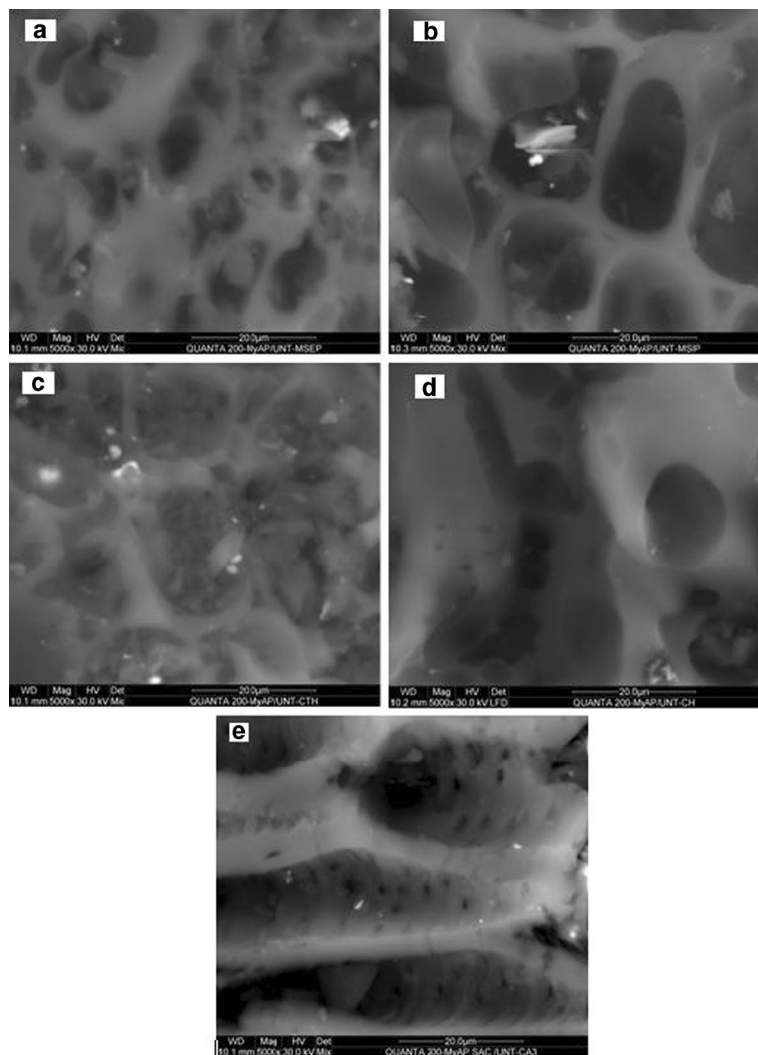
images, specifically the white material on the activated carbon surface. This originates from the chemical activator and other activation and pyrolysis by-products.

3.3 Adsorption Experiments

The overall order in adsorption performance of activated carbons produced with respect to the rate of adsorption process (the rate constants k_2) was as follows: CC-AC> CPH-AC>MSEP-AC≈MSIP-AC≈CH-AC (see Fig. 6a). The best adsorption performance of CC-AC may be explained based on two factors: (1) the mesoporosity and (2) the size selectivity of the micropores and mesopores with respect to dimensions of methylene blue molecule.

The mesoporosity (i.e., the structure of mesopores) plays an important role concerning the transport of the MB molecules to micropores. From this point of view, the mesopore size distribution of ACs can be correlated with the improved adsorption ability of ACs. From Fig. 3d–f, the slit-shaped mesopore size distributions of individual activated carbons can be compared. It is evident that the mesopores of CC-AC show more uniform and larger sizes than for other activated carbons, which probably arises from the porosity of the raw agromaterial. This fact also corresponds with the SEM results shown in Fig. 5a–e, where the porous structure of CC-AC (Fig. 5e) is the most channel-like. The mesopore size distributions of other activated carbons are more similar to each other; but mostly CPH-AC to CH-AC and MSEP-AC to MSIP-AC. The higher population of smaller mesopores is present in MSEP-AC and MSIP-AC. Considering the molecular dimensions of MB from our estimation via DFT calculations (1.66×0.82× 0.54 nm; Fig. 7), it seems that MB will diffuse and adsorb the most likely in mesopores of CC-AC. Since

mesopore size distributions of other activated carbons are quite similar (Fig. 3d, e), the transport of MB within the mesoporous structure will be more or less similar, resulting thus to a similar adsorption behavior.

Secondly, the size selectivity of the micropores with respect to dimensions of methylene blue molecule is also the factor which must be considered. It can be reasonably supposed that the adsorption of MB cannot occur on the whole micropore surface of the activated carbons. This assumption is in agreement with molecular simulations of MB. It is evident from Fig. 7 that MB due to its dimensions may be adsorbed only in larger micropores (with pore size>0.54 nm) in all ACs. From Table 5, it is evident that CPH-AC shows the highest micropore volume. Since all ACs possess practically the same micropore size distribution (Fig. 4), however, CPH-AC possess the highest micropore volume of 322 mm^3_{liq}/g (Table 4), the highest adsorption within the micropores can be expected for CPH-AC. Based on all the above mentioned facts, it seems that the best adsorption performance for MB on CC-AC and CPH-AC can be attributed to the well-developed mesoporous structure of CC-AC showing the highest mesopore surface area, and when the mesopore surface areas of ACs are similar, than to the contribution of available micropore volume which is the highest for CPH-AC.

According to the pseudo-second order kinetic model (Eq. 3), t/q_t was plotted as a function of time, giving the linear correlations within all the experimental results (Fig. 6b). The second-order adsorption rate constants (k_2) and the equilibrium adsorption capacities (q_e) were obtained from the slopes and the intercepts and are summarized together with the values of the correlation coefficients R^2 in Table 5. It is obvious from Table 5 that although the equilibrium adsorption capacity of investigated ACs for MB is decreasing in the ranking MSEP-

Fig. 6 **a** Removal of methylene blue using the individual activated carbons produced. **b** Pseudo-second-order kinetic plots for methylene blue adsorption by activated carbons produced
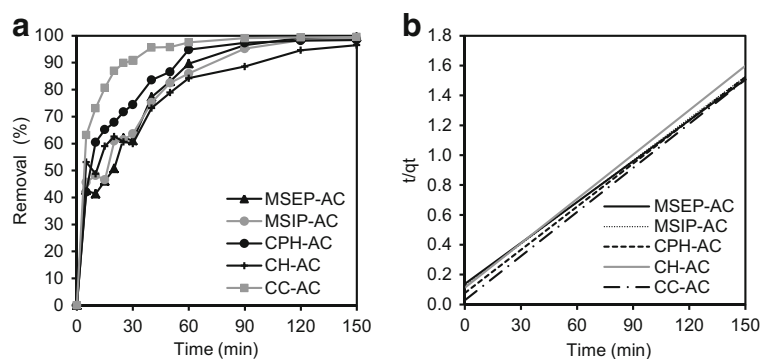
Fig. 7 The contour map of electrostatic potential in *xy*-axis and *xz*-axis planes of methylene blue. The *bold blue line* corresponds to the vdW surface (isosurface of electron density= 0.001 a.u.). 1 bohr=0.529 Å
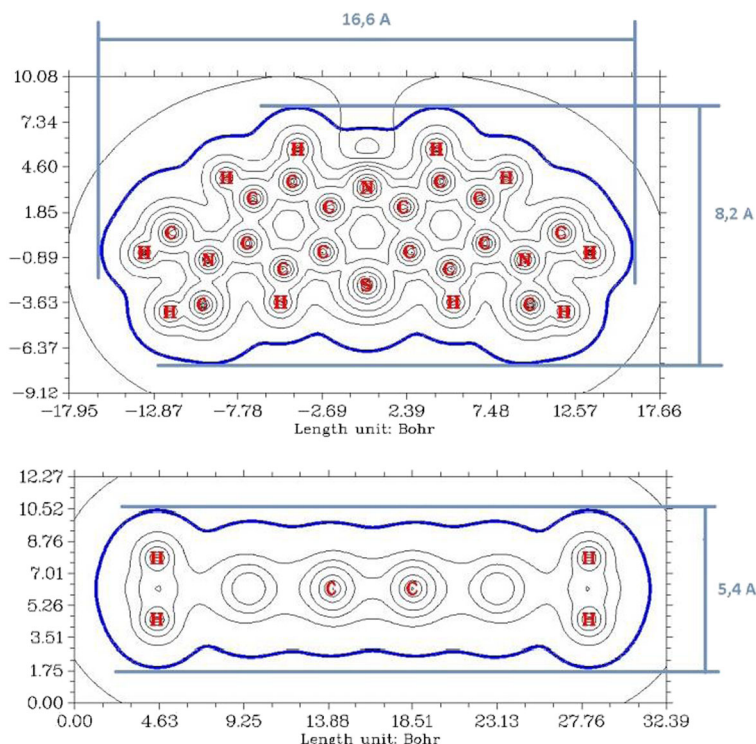
AC>MSIP-AC>CPH-AC>CC-AC>CH-AC, the difference between ACs is only within a thinny range of 100–110 mg_{MB}/g_{AC} (i.e., within 10 %). The adsorption of MB proceeded the most feasibly on CC-AC (k_2= 0.0034 g/mg min) followed by CPH-AC (k_2=0.0012 g/ mg min). The MB adsorption on other ACs (MSEP-AC, MSIP-AC, and CH-AC) proceeded comparably (k_2~ 0.0006–0.0009 g/mg min). The correlation coefficients R^2 (Table 5) indicate that CC-AC (0.9995) and CPH-AC (0.9956) are the activated carbons that fit best the pseudo-second kinetic model. Significantly more feasible MB adsorption on CC-AC and CPH-AC pretty corresponds

to the discussed textural observations that the better-developed mesoporous structure of CC-AC (i.e., pore size distribution) showing a significantly higher mesopore surface area, and the largest contribution of micropores surface of CPH-AC, when the mesoporous structure of ACs are comparable, play the key role in the MB adsorption.

The fact that the activated carbons perfectly follow the pseudo-second-order model shows that the adsorption between adsorbate and adsorbent is chemical in nature. Chemisorption involves valence forces through sharing or exchange of electrons between the sorbent and the sorbate (Ho and Mckay 1999). Thus, the different equilibrium adsorption capacities of investigated ACs may be a consequence of different surface properties (e.g., functional groups such as carbonyl or carboxyl groups which may be present).

Table 5 Pseudo-second-order kinetic constants for methylene blue adsorption

Activated carbon	R^2	q_e (mg/g)	k_2 (g/mg·min)	h (g/mg·min)
MSEP-AC	0.9814	110	0.0006	7.23
MSIP-AC	0.9859	106	0.0007	8.10
CPH-AC	0.9956	104	0.0012	13.12
CH-AC	0.9858	101	0.0009	8.96
CC-AC	0.9995	102	0.0034	35.84

4 Conclusions

Activated carbons were prepared from a broad range of agro-industrial wastes (five different types), including one novel raw agro-material in the activated carbon production—external part of the mango pit (mango seed husk, MSEP-RM).

The raw agro-materials used exhibited porous structures possessing very low surface areas and with porosities within the broad range of 0.29–0.44 m^2/g and 15–65 %, respectively. CC-RM was the most porous material ($\varepsilon = 65 \pm 1$ %), showing dominantly uniform macropores of large volume. Other raw materials showed a wide range of pore sizes.

Despite the different porosity of individual raw materials, all activated carbons produced demonstrated well-developed microporous–mesoporous structure. Among others, CC-AC and CPH-AC were the special cases. CC-AC showed significantly higher mesopore surface area (~618 m^2/g) than other ACs (503–561 m^2/g), but not so high micropore volume. CPH-AC showed the highest micropore volume from all produced ACs. Micropore size distributions of ACs were similar. Concerning the mesopore size distributions, CC-AC comprised the most uniform and wide channel-like mesopores. Based on textural analyses, it was revealed that the pore size distribution of the raw agro-material is a more important property in developing of microporous–mesoporous structure of ACs than their overall porosity. It affects the level of interaction of an activation agent with a lignocellulosic material.

All produced ACs were investigated in the removal of methylene blue, as a representative large molecular size organic pollutant, in aqueous phase. It was revealed that the mesoporosity and the ratio of micropores accessible for MB are the determining factors in the MB adsorption since there exists the size-selectivity effect for MB due to its molecular dimensions. The molecular dimensions of MB were estimated in this study via DFT calculations to be $1.66 \times 0.82 \times 0.54$ nm. The most feasible adsorption of MB on CC-AC and CPH-AC is explained based on the well-developed mesoporous structure of CC-AC, and the largest contribution of accessible micropores of CPH-AC while being mesoporous structure of ACs comparable. MB adsorption data were fitted well to the pseudo-second-order kinetic model.

Conflict of Interest   The authors declare that they have no conflict of interest.

References

Ahmad, M. A., & Rahman, N. K. (2011). Equilibrium, kinetics and thermodynamic of remazol brilliant orange 3R dye adsorption on coffee husk-based activated carbon. *Chemical Engineering Journal, 170*(1), 154–161.

Ahmad, F., Daud, W. M. A. W., Ahmad, M. A., & Radzi, R. (2012). Cocoa (*Theobroma cacao*) shell-based activated carbon by CO$_2$ activation in removing of cationic dye from aqueous solution: kinetics and equilibrium studies. *Chemical Engineering Research and Design, 90*(10), 1480–1490.

Ahmadpour, A., & Do, D. D. (1997). The preparation of activated carbon from macadamia nutshell by chemical activation. *Carbon, 35*(12), 1723–1732.

Akpen, G. D., Nwaogazie, I. L., & Leton, T. G. (2011). Optimum conditions for the removal of colour from waste water by mango seed shell based activated carbon. *Indian Journal of Science and Technology, 4*(8), 890–894.

Azevedo, D., Araujo, J., Bastos-Neto, M., Torres, A. E. B., Jaguaribe, E. F., & Cavalcante, C. L. (2007). Microporous activated carbon prepared from coconut shells using chemical activation with zinc chloride. *Microporous and Mesoporous Materials, 100*(1), 361–364.

Bagheri, N., & Abedi, J. (2009). Preparation of high surface area activated carbon from corn by chemical activation using potassium hydroxide. *Chemical Engineering Research and Design, 87*(8), 1059–1064.

Barrett, P. E., Joyner, L. G., & Halenda, P. P. (1951). The determination of pore volume and area distributions in porous substances—computations from nitrogen isotherms. *Journal of the American Chemical Society, 73*, 373–380.

Becke, A. D. J. (1993). Density functional thermochemistry. III. The role of exact exchange. *Chemical Physics, 98*, 5648–5652.

Bekalo, S. A., & Reinhardt, H. W. (2010). Fibers of coffee husk and hulls for the production of particle board. *Materials and Structures, 43*, 1049–60.

Bello, O., Ahmad, M., & Siang, T. (2011). Utilization of cocoa pod husk for the removal of Remazol Black B reactive dye from aqueous solutions: kinetic, equilibrium and thermodynamic studies. *Trends in Applied Sciences Research, 6*, 794–812.

Brunauer, S., Emmett, P. H., & Teller, E. (1938). Adsorption of gases in multimolecular layers. *Journal of the American Chemical Society, 60*, 309–319.

Cruz, G., Pirilä, M., Huuhtanen, M., Carrión, L., & Alvarenga, E. (2012). Production of activated carbon from cocoa (*Theobroma cacao*) pod husk. *Journal Civil Environmental Engineering, 2*(109), 1–6.

Dias, J. M., Alvim-Ferraz, M., Almeida, M. F., Rivera-Utrilla, J., & Sánchez-Polo, M. (2007). Waste materials for activated carbon preparation and its use in aqueous-phase treatment: a review. *Journal of Environmental Management, 85*(4), 833–846.

Elizalde-González, M. P., & Hernandez-Montoya, V. (2007). Characterization of mango pit as raw material in the preparation of activated carbon for wastewater treatment. *Biochemical Engineering Journal, 36*(3), 230–238.

Fisal, A., Daud, W. M. A. W., Ahmad, M. A., & Radzi, R. (2011). Using cocoa (*Theobroma cacao*) shell-based activated carbon to remove 4-nitrophenol from aqueous solution: kinetics and equilibrium studies. *Chemical Engineering Journal, 178*, 461–467.

Frisch, M., Trucks, G. W., Schlegel, H., Scuseria, G. E., Robb, M. A., Cheeseman, J. R., & Dannenberg, J. J. (2004). *Gaussian 03, revision c. 02* (p. 4). Wallingford: Gaussian. Inc.

Galiatsatou, P., Metaxas, M., & Kasselouri-Rigopoulou, V. (2001). Mesoporous activated carbon from agricultural byproducts. *Mikrochimica Acta, 136*, 147–152.

Gregg, S. J., & Sing, K. S. W. (1982). *Adsorption, surface area and porosity*. New York: Academic Press.

Hatta, Z. M. (2013). Chemical composition and morphological of cocoa pod husk and cassava peels for pulp and paper production. *Australian Journal of Basic and Applied Sciences, 7*(9), 406–411.

Ho, Y. S., & McKay, G. (1999). Pseudo-second order model for sorption processes. *Process Biochemistry, 34*(5), 451–465.

Horvath, G., & Kawazoe, K. (1983). Method for the calculation of effective pore size distribution in molecular sieve carbon. *Journal of Chemical Engineering of Japan, 16*(6), 470–475.

Hu, Z., Guo, H., Srinivasan, M. P., & Yaming, N. (2003). A simple method for developing mesoporosity in activated carbon. *Seperation and Purification Technology, 31*, 47–52.

Kwaghger, A., & Ibrahim, J. S. (2013). Optimization of conditions for the preparation of activated carbon from mango nuts using HCl. *American Journal of Engineering Research, 2*(7), 74–85.

Lecloux, A., & Pirard, J. P. (1979). The importance of standard isotherms in the analysis of adsorption isotherms for determining the porous texture of solids. *Journal of Colloid and Interface Science, 70*(2), 265–281.

Lee, C. T., Yang, W. T., & Parr, R. G. (1988). Development of the Colle–Salvetti correlation-energy formula into a functional of the electron-density. *Physical Review B, 37*, 785–789.

Liou, T. H. (2010). Development of mesoporous structure and high adsorption capacity of biomass-based activated carbon by phosphoric acid and zinc chloride activation. *Chemical Engineering Journal, 158*, 129–142.

Lu, T., & Chen, F. (2012). Multiwfn: a multifunctional wave function analyzer. *Journal of Computational Chemistry, 33*, 580–592.

Minagri- Ministry of Agriculture and Drainage of Peru (2013). Agricultural dynamic 2003 – 2012. http://www.minag.gob.pe/portal/download/pdf/especiales/dinamica/dinamicaagropecuaria2003-2012.pdf. Accessed 4th of August 2014.

Mohan, D., Pittman, C. U., & Steele, P. H. (2006). Pyrolysis of wood/biomass for bio-oil: a critical review. *Energy and Fuels, 20*(3), 848–889.

Nieto-Delgado, C., & Rangel-Mendez, J. R. (2013). In situ transformation of agave bagasse into activated carbon by use of an environmental scanning electron microscope. *Microporous and Mesoporous Materials, 167*, 249–253.

Oliveira, L. C., Pereira, E., Guimaraes, I. R., Vallone, A., Pereira, M., Mesquita, J. P., & Sapag, K. (2009). Preparation of activated carbons from coffee husks utilizing $FeCl_3$ and $ZnCl_2$ as activating agents. *Journal of Hazardous Materials, 165*(1), 87–94.

Roberts, B. F. (1967). A procedure for estimating pore volume and area distributions from sorption isotherms. *Journal of Colloid and Interface Science, 23*(2), 266–273.

Schneider, P. (1995). Adsorption isotherms of microporous–mesoporous solids revisited. *Applied Catalysis A: General, 129*(2), 157–165.

Song, M., Jin, B., Xiao, R., Yang, L., Wu, Y., Zhong, Z., & Huang, Y. (2013). The comparison of two activation techniques to prepare activated carbon from corn cob. *Biomass and Bioenergy, 48*, 250–256.

Sun, Y., & Webley, P. A. (2010). Preparation of activated carbons from corncob with large specific surface area by a variety of chemical activators and their application in gas storage. *Chemical Engineering Journal, 162*(3), 883–892.

Sych, N. V., Trofymenko, S. I., Poddubnaya, O. I., Tsyba, M. M., Sapsay, V. I., Klymchuk, D. O., & Puziy, A. M. (2012). Porous structure and surface chemistry of phosphoric acid activated carbon from corncob. *Applied Surface Science, 261*, 75–82.

Theivarasu, C., & Mylsamy, S. (2010). Equilibrium and kinetic adsorption studies of Rhodamine-B from aqueous solutions using cocoa (*Theobroma cacao*) shell as a new adsorbent. *International Journal of Engineering Science and Technology, 2*(11), 6284–6292.

Tsai, W. T., Chang, C. Y., & Lee, S. L. (1998). A low cost adsorbent from agricultural waste corn cob by zinc chloride activation. *Bioresource Technology, 64*(3), 211–217.